

UWB Pulse Decomposition in Simple Printed Structures

Alexander Talgatovich Gazizov, Alexander Mikhailovich Zabolotsky, and Talgat Rashitovich Gazizov

Abstract—The paper describes the ultra-wideband (UWB) pulse decomposition in simple printed structures aimed at low-cost and effective protection. The structure of an asymmetrical modal filter without resistors is considered, and the possibility of the attenuation by a factor of 55 is shown. Another structure—a turn of a meander line (ML)—is described, and the possibility of the attenuation by a factor of 2.5 is shown. Simulations without and with frequency-dependent losses in conductors and dielectrics are compared with experimental results. Based on the described principles, new devices can be designed which will be reliable, cheap, and radiation resistant due to the absence of any lumped components.

Index Terms—Coupled transmission lines, protection, time-domain analysis.

I. INTRODUCTION

NOWADAYS, there exists an increasing threat of deliberate electromagnetic impact on electronics [1]. Such an impact can result in malfunction or failure of electronic equipment. Impact of ultra-wideband (UWB) pulses is particularly dangerous, because existing surge protectors do not protect against it [2], [3]. Known industrial devices, which protect against UWB pulses, have large dimensions and high cost. Thus, currently, there is no, both low-cost and effective, protection against UWB pulses. However, the increasing role of electronics in our life makes this protection essential. Therefore, the search for new design principles of the protection against UWB pulses is important.

The idea of modal filtration has been suggested in [4], and several devices based on modal filtration principle have been developed, including symmetrical structures of modal filters (MF) for Fast Ethernet network [5], for lightning [6] and electrostatic discharge [7] protection. The physical principle of their operation is based on the phenomenon of the UWB pulse decomposition into modes with different propagation delays in the coupled line. The difference between these delays can be longer

Manuscript received November 11, 2015; revised February 21, 2016; accepted March 24, 2016. Date of publication April 20, 2016; date of current version July 22, 2016. Development of necessary software was supported by the state Contract 8.1802.2014/K of the Russian Ministry of Education and Science, modeling of coupled lines was supported by RFBR Grant 14-29-0925, and simulation of waveforms was carried out at the expense of RSF Grant 14-19-01232 in TUSUR University.

A. T. Gazizov is with the National Research Tomsk Polytechnic University, Tomsk 634050, Russia and also with Tomsk State University of Control Systems and Radioelectronics, Tomsk 634050, Russia (e-mail: alexandr.bbm@gmail.com).

A. M. Zabolotsky and T. R. Gazizov are with Tomsk State University of Control Systems and Radioelectronics, Tomsk 634050, Russia (e-mail: zabolotsky_am@mail.ru; talgat@tu.tusur.ru).

Color versions of one or more of the figures in this paper are available online at <http://ieeexplore.ieee.org>.

Digital Object Identifier 10.1109/TEMC.2016.2548783

than the duration of the interference pulse if there is a non-homogeneous dielectric filling in the cross section of the line. One pulse applied between the active and reference conductors at the near end of the line will be decomposed into two pulses at the far end of the line.

The asymmetrical MF based on the PCB technology has been considered recently, and it has been shown that this MF with special resistors can attenuate the UWB pulse by a factor of [7], [8]. Recent research showed that it is important to investigate the structures without resistors in order to reduce cost of the device and to make a protective structure in itself a thin strip of foiled fiberglass that can decompose dangerous pulses. Using this idea preliminary investigations of the MF without resistors were carried out in [9]–[11]. Another simple structure that is worth studying is a meander line (ML) (or coupled C-section), which has many applications [12] and has been considered as a protective device recently [13], [14]. However, previous investigations include only preliminary lossless simulation without experimental confirmation of simulation. The aim of this paper is to summarize obtained results and to present the simulation accounting losses as well as preliminary experimental results confirming the validity of the simulation.

II. RESEARCH METHOD

In order to investigate the structures, the numerical simulation is used. Simulation of electrical characteristics is often carried out using the electromagnetic analysis. However, for long, two-dimensional (2-D) structures a quasi-static approach is often relevant. Particularly, it allows obtaining causal results taking into account frequency-dependent losses in conductors and dielectrics [15]. In this paper, we use TALGAT software [16], which is designed for computer simulation of a wide class of problems of electromagnetic compatibility by performing the following main functions: quasi-static analysis (calculation of matrices) of arbitrary 2-D and three-dimensional (3-D) structures of conductors and dielectrics; electromagnetic analysis of arbitrary 3-D wire structures; computation of time and frequency responses of multiconductor transmission lines; and structural and parametric optimization.

The simulation of the UWB pulse propagation is carried out by a quasi-static analysis based on fast and accurate models [17] implemented in TALGAT software. A coupled line is a basis for proposed structures. It is assumed in the analysis that a coupled line is uniform along its length with an arbitrary cross section. In the general case, the cross section with N_{cond} signal conductors and a reference one is represented by the following $N_{\text{cond}} \times N_{\text{cond}}$ matrices of line per-unit-length parameters: inductance (\mathbf{L}), coefficients of electrostatic induction (\mathbf{C}),

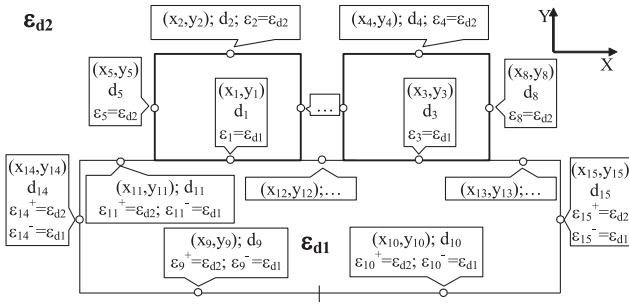


Fig. 1. Segmentation of two-dimensional configuration boundaries.

resistance (\mathbf{R}), conductance (\mathbf{G}). In paper [18] an approach based on a modified nodal admittance matrix has been presented for the formulation of network equations including the coupled transmission line, terminal, and interconnecting networks. Voltages in the time domain are obtained by applying the inverse fast Fourier transform. Matrices \mathbf{L} , \mathbf{C} , and \mathbf{G} are calculated by a method of moments. The mathematical model for the considered case of linear and orthogonal boundaries of conductors and dielectrics [19] implemented in TALGAT software is described later.

A. Calculation of the Capacitance Matrix

An example geometry of a cross section with finite ground (two conductors on a dielectric substrate) and its segmentation principle are shown in Fig. 1. First, we segment conductor–dielectric boundaries which are orthogonal to the Y -axis (the serial number of the last subinterval is Nc_Y). Then, we segment conductor–dielectric boundaries which are orthogonal to the X -axis (the serial number of the last subinterval is Nc). After that, we segment dielectric–dielectric boundaries which are orthogonal to the Y -axis (the serial number of the last subinterval is Nd_Y) and finally segment dielectric–dielectric boundaries which are orthogonal to the X -axis (the serial number of the last subinterval is N).

Each n th subinterval has the following parameters: x_n is the x -coordinate of the center; y_n is the y -coordinate of the center; d_n is the length; ε_n is the permittivity for conductor–dielectric subintervals; ε_n^+ and ε_n^- are the permittivities for dielectric–dielectric subintervals on the positive and negative sides of the boundary relative to X - or Y -axis. The parameters are used to calculate the entries of the matrix of the linear system to be solved.

For the matrix rows with numbers $m = 1, \dots, Nc$, we have

$$S_{mn} = -\frac{I_{mn}}{2\pi\varepsilon_0}, \begin{cases} m=1, \dots, Nc \\ n=1, \dots, N \end{cases}$$

where

$$I_{mn} = a_1 \cdot \ln(a_1^2 + c_1^2) - 2a_1 + 2c_1 \cdot \arctg\left(\frac{a_1}{c_1}\right) - a_2 \cdot \ln(a_2^2 + c_1^2) + 2a_2 - 2c_1 \cdot \arctg\left(\frac{a_2}{c_1}\right).$$

For $n = 1, \dots, Nc_Y, (Nc + 1), \dots, Nd_Y$

$$a_1 = \frac{d_n}{2} - (x_m - x_n); \quad a_2 = \frac{-d_n}{2} - (x_m - x_n);$$

$$c_1 = y_m - y_n. \quad (1)$$

For $n = (Nc_Y + 1), \dots, Nc, (Nd_Y + 1), \dots, N$

$$a_1 = \frac{d_n}{2} - (y_m - y_n); \quad a_2 = \frac{-d_n}{2} - (y_m - y_n);$$

$$c_1 = x_m - x_n. \quad (2)$$

For the matrix rows with numbers $m = (Nc + 1), \dots, N$, we have

$$S_{mn} = \frac{I_{mn}}{2\pi\varepsilon_0} \begin{cases} m=(Nc+1), \dots, N \\ n=1, \dots, N \end{cases}, \quad m \neq n;$$

$$S_{mm} = \frac{I_{mm}}{2\pi\varepsilon_0} + \frac{1}{2\varepsilon_0} \frac{\varepsilon_m^+ + \varepsilon_m^-}{\varepsilon_m^+ - \varepsilon_m^-}, \quad m = (Nc + 1), \dots, N$$

where for the matrix rows with numbers $m = (Nc + 1), \dots, Nd_Y$, for $n = 1, \dots, Nc_Y, (Nc + 1), \dots, Nd_Y$

$$I_{mn} = \arctg\left(\frac{a_1}{c_1}\right) - \arctg\left(\frac{a_2}{c_1}\right) \quad (3)$$

and the variables coincide with those defined by (1), while for $n = (Nc_Y + 1), \dots, Nc, (Nd_Y + 1), \dots, N$, we have

$$I_{mn} = \frac{1}{2} \ln\left(\frac{a_2^2 + c_1^2}{a_1^2 + c_1^2}\right) \quad (4)$$

where the variables coincide with those defined by (2). For the matrix rows with numbers $m = (Nd_Y + 1), \dots, N$, for $n = 1, \dots, Nc_Y, (Nc + 1), \dots, Nd_Y$, the I_{mn} is calculated from (4) with variables defined by (1). For $n = (Nc_Y + 1), \dots, Nc, (Nd_Y + 1), \dots, N$, I_{mn} is calculated from (3) with the variables coinciding with those defined by (2).

In the considered case, where the infinite ground plane is absent and the $(N\text{cond} + 1)$ th conductor is grounded, we follow the paper [21] and add $(N + 1)$ th row and column with entries defined by

$$S_{nN+1} = \frac{d_n}{2S_{nn}}$$

$$S_{N+1n} = d_n \varepsilon_n, \quad n = 1, \dots, Nc.$$

The linear system to be solved assumes the form

$$\sum_{n=1}^N S_{mn} \sigma_n = \begin{cases} V_i, & m=1, \dots, Nc \\ 0, & m=(Nc+1), \dots, N. \end{cases}$$

The subscript i here means that each segment belonging to the i th conductor has the potential required for the determination of the capacitance matrix. The entries S_{mn} are gathered together and yield the square matrix \mathbf{S} relating the charge densities on segments of conductor and dielectric boundaries, forming the vector σ , with the potentials of these segments forming the vector \mathbf{V} . Thus, the problem itself is expressed in the form of the compact linear system $\mathbf{S}\sigma = \mathbf{V}$, which is solved $N\text{cond}$ times. In the i th solution, the conductor potential V_i , $i = 1, \dots, N\text{cond}$, is set equal to 1 V, while the potentials of all remaining

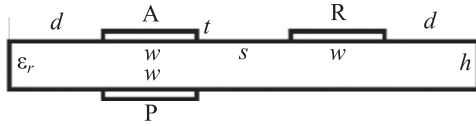


Fig. 2. Cross section of proposed structures.

conductors are set equal to 0 V. Finally, from the definition of the entry of the capacitance matrix, we obtain

$$C_{ij} = \sum_{n=NF_i}^{NL_i} \frac{\epsilon_n}{\epsilon_0} \sigma_n^{(j)} d_n, \quad i, j = 1, \dots, N \text{ cond.}$$

Here NF_i and NL_i are the numbers of the first and the last subintervals of the i th conductor, the subscript i denotes the conductor for which charges $\sigma_n^{(i)}$ are summed, and the superscript j indicates the serial number of σ_n calculated when the potential of the j th conductor is set equal to 1 V and the potentials of the remaining conductors are set equal to 0 V.

B. Cross Section and Simulation Parameters

Cross section of proposed structures is shown in Fig. 2. Initially, it has optimal parameters obtained in the previous paper [8]: separation of conductors $s = 15$ mm; width of conductors $w = 15$ mm; dielectric thickness $h = 0.5$ mm; thickness of conductor $t = 105$ μm ; distance between the edge of the structure and the conductor $d = w$; and relative permittivity $\epsilon_r = 4$. Pulse signal is excited between the active (A) and reference (R) conductors (see Fig. 2). EMF source parameters: rise, top, and fall times $t_r = t_f = t_d = 1$ ns, while the amplitude is 2 kV.

First, the calculation of the time response is performed in a lossless approximation when per-unit-length conductance (\mathbf{G}) and resistance (\mathbf{R}) matrices are equal to zero matrix. For more accurate evaluation of the amplitudes of the decomposed pulses, the simulation with losses in dielectrics and conductors is carried out. The losses for the defined frequency are completely defined by matrices \mathbf{R} and \mathbf{G} . The frequency dependence of these matrices is considered.

The frequency dependence of the complex FR-4 permittivity is taken into account by analytical models for complex dielectric constants from [15]. Using the constants, the complex capacitance matrix \mathbf{C} is obtained, and the conductance matrix \mathbf{G} is derived from imaginary part of \mathbf{C} as described in [20].

The entries of the matrix \mathbf{R} are calculated taking into account the skin effect but without consideration of the proximity effect. All conductors have the same cross section; therefore, diagonal (r) and nondiagonal (r_m) entries of the matrix \mathbf{R} are related by the expression $r = 2 r_m$, where $r_m = 1/(w\sigma t) + r_s/w$, σ is the copper conductivity, $r_s = (\pi f \mu_0 / \sigma)^{1/2}$, f is the frequency, and μ_0 is the free space permeability.

III. ASYMMETRICAL MF

A. Initial Structure of MF

The MF circuit diagram is shown in Fig. 3: the length $l = 1$ m; U_1 – U_5 are the nodes; R_e is the EMF source resistance; R_L is the

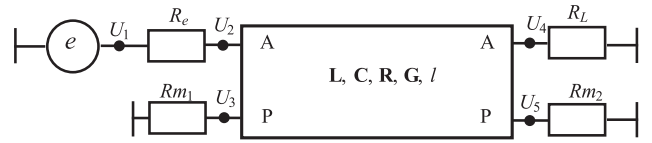


Fig. 3. Circuit diagram of the connected MF.

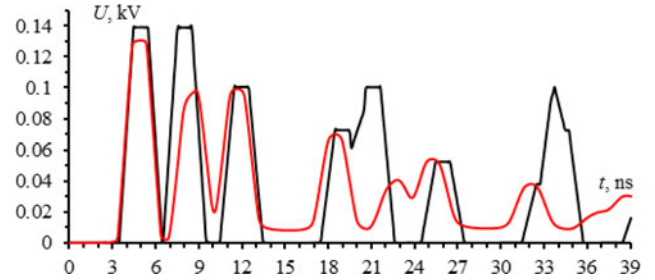


Fig. 4. Output waveforms of the MF for the “matched” case with (—) and without (---) losses. Lossless waveform is adapted from [10].

load resistance; $R_{m1,2}$ are the MF resistances; A-A is the active conductor, and P-P is the passive conductor. Previously, it was supposed that the amplitudes of the decomposed pulses were at a minimum when all the resistances were equal to geometric mean of the even and odd modes impedances (“matched” case) [22]. This condition makes the amplitudes equal and also decreases reflections. In this case, $R_e = R_L = R_{m1,2} = R = 36.515 \Omega$.

The output (U_4 in Fig. 3) waveform of the MF for the “matched” case with and without losses is shown in Fig. 4. Let us consider the waveform according to the modal theory. The first pulse corresponds to the even mode which propagates mostly in the air. Therefore, its arrival time t_e can be estimated as $t_e \approx l/c = 3.3$ ns, where l is the length of MF and c is the speed of light in vacuum. Per-unit-length delay of the even mode τ_e calculated in TALGAT software is 3.49 ns/m and the arrival time of the first pulse for $l = 1$ m is 3.49 ns, which coincides with that from Fig. 4. The second pulse arrives later as it corresponds to the odd mode, which propagates mostly in the dielectric substrate. The arrival time of the odd mode t_o can be estimated as $t_o \approx t_e \cdot \sqrt{\epsilon_r} = 6.6$ ns. The calculated arrival time of the odd mode t_o is 6.54 ns, which similarly corresponds to Fig. 4. Other pulses are reflections of the first two pulses: the arrival time of the i th pulse of the particular mode can be calculated as $t_i = t_{e,o}(1 + 2i)l$. For example, arrival times of pulses corresponding to the even mode are 10.5, 17.5, and 24.4 ns. Thus, the obtained waveform (see Fig. 4) validates presented analytical estimations and calculations.

Let us analyze the output amplitude of the MF. In the case without losses, the amplitude is defined by first two pulses and is equal to 0.14 kV and the attenuation coefficient is 7 (relative to 1 kV). Taking into account the losses, the odd mode (second pulse) decreases by 0.05 kV (1.56 times) because it propagates mostly in the FR-4 and undergoes the dielectric losses. However, the even mode (first pulse) decreases only by 0.01 kV (1.077 times), as it propagates mostly in the air. Thus, the resulting amplitude of the waveform with consideration of losses

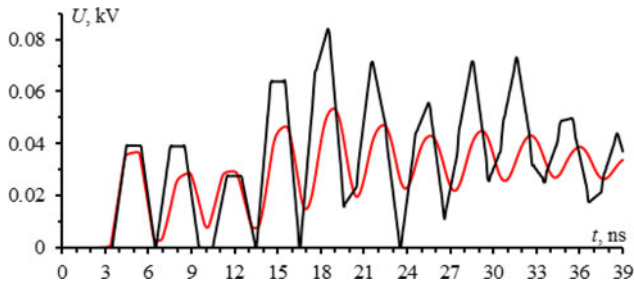


Fig. 5. Output waveforms of the MF without resistors with (—) and without (—) losses. Lossless waveform is adapted from [10].

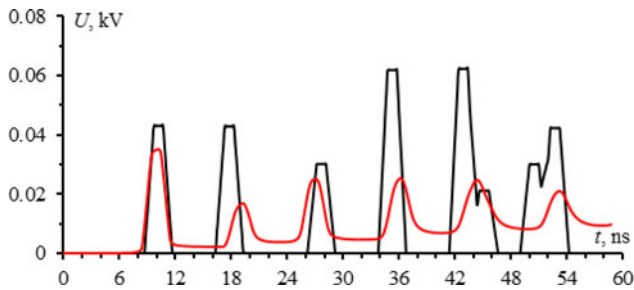


Fig. 6. Output waveforms of the MF ($l = 2.5$ m, $\epsilon_r = 4$) without resistors with (—) and without (—) losses. Lossless waveform is adapted from [10].

has decreased slightly. However, reflections are attenuated more considerably.

B. MF Without Resistors

In order to simulate the MF without resistors, Rm_1 and Rm_2 should have limit values corresponding to the open-circuit and the short-circuit modes. Waveforms at the output of the MF were calculated for different combinations of limit values of Rm_1 and Rm_2 . The highest attenuation coefficient was obtained in the case when one of the resistors was simulated in the open-circuit mode and another in the short-circuit. It was revealed that the order of resistors does not influence the output waveform. Waveform at the output of the MF with $Rm_1 = 1000R$ and $Rm_2 = 0.001R$ is shown in Fig. 5. The obtained waveform without losses shows that the amplitude is 0.084 kV and that the attenuation coefficient is 12. With consideration of losses, the amplitude is 0.053 kV and the attenuation coefficient is equal to 19. Thus, the resulting influence of losses in this case is more considerable. It is explained by the fact that the amplitude is now defined not by the first travelling wave pulse but by the following components undergoing several reflections and therefore attenuating more considerably.

In Fig. 5, the amplitude is defined not by the first pulse, as in Fig. 4, but by the fifth pulse. The fifth pulse in Fig. 5 is a superposition of two pulses and its amplitude can be reduced by changing the parameters of the structure. For example, we can increase the length of the MF in order to increase the time interval between pulses.

The output waveform of the MF with an increased length ($l = 2.5$ m) is shown in Fig. 6. Arrival times of pulses with

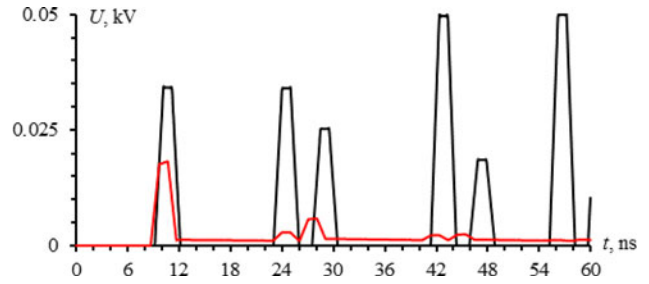


Fig. 7. Output waveform of the MF ($l = 2.5$ m, $\epsilon_r = 8$) with (—) and without (—) losses. Lossless waveform is adapted from [10].



Fig. 8. Manufactured MF.

increased length have been proportionally increased. Note that the amplitude of the fifth pulse without losses decreases down to 0.062 kV (attenuation coefficient increases to 16), because the fifth pulse is no longer a complete superposition of the two pulses.

With the increase of the length of the structure, the influence of losses becomes more significant because reflections pass a longer way: the amplitude is actually defined by the first pulse and is equal to 0.035 kV. Attenuation coefficient is 29, that is, almost twice better than without consideration of losses.

However, the amplitude can be further decreased by increasing the ϵ_r value which previously was equal to 4, according to the dielectric substrate material (cheap and widely used FR-4). The output waveform of the MF with increased l and ϵ_r values is shown in Fig. 7, where the amplitude without losses is 0.05 kV and attenuation coefficient is 20. Simulation with losses in this case (see Fig. 7) is carried out without frequency dependence of dielectric permittivity. The losses reduce the amplitude down to 0.018 kV and increase the attenuation coefficient up to 55.

IV. COMPARISON OF EXPERIMENT AND SIMULATION

To validate the simulation used, the experiment is performed. For this purpose, we use the initial structure of the MF with resistors which has other geometrical parameters for the simplicity of the experiment.

The manufactured MF (see Fig. 8) of the same cross section is made of the double-sided foiled fiberglass and has the following geometrical parameters: $s = 4$ mm, $w = 3$ mm, $h = 0.18$ mm, $t = 65$ μ m, $d = w$, and $l = 0.2$ m. Resistors $Rm_1 = Rm_2 = 50$ Ω are chosen to match the line. SMA connectors are soldered to the input and output of the device in order to connect it into a 50 Ω measuring tract.

The input waveform is an approximately triangular UWB pulse with the amplitude of 600 mV (on 50 Ω load) and the duration of 820 ps (at level 0.1). The experimental input waveform is shown in Fig. 9. The experimental output waveform of the MF is shown in Fig. 10.

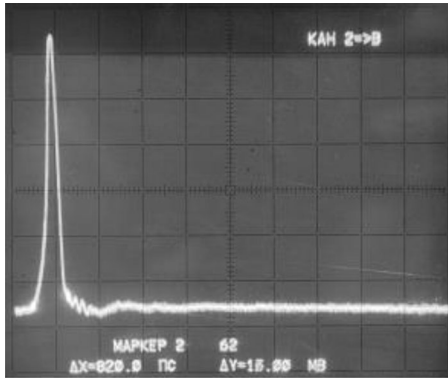


Fig. 9. Input waveform oscillogram. Time and voltage scales—1 ns/div and 0.1 V/div.

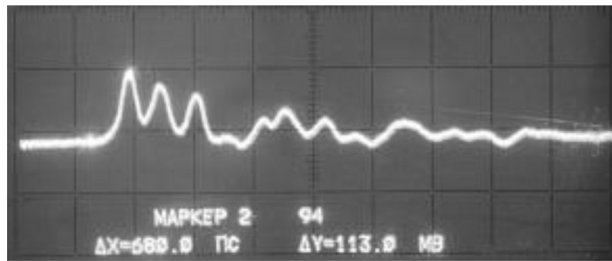


Fig. 10. MF output waveform oscillogram. Time and voltage scales are 1 ns/div and 0.1 V/div, respectively.

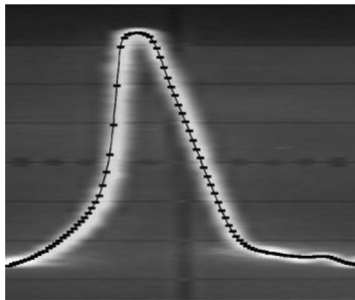


Fig. 11. Horizontally enlarged image of the experimental output waveform (white curve) and its digitized form for the simulation (black curve).

As a result of the modal distortion, the amplitudes of output pulses (see Fig. 10) are 113 mV (first pulse) and 91 mV (second pulse), other pulses are dumping reflections. The difference of propagation delays of the first two pulses is approximately 0.6 ns. The output amplitude is about six times smaller than the amplitude of the input pulse.

The simulation of the UWB pulse propagation taking into account the losses for the same structure of MF is performed using TALGAT software and methods described above. In order to simulate the input signal with high accuracy, we digitize the experimental input waveform and set it as a user-defined pulse source in TALGAT software (see Fig. 11). The simulated output waveform of the MF is shown in Fig. 12.

According to the simulation, the amplitudes of output pulses are 100 mV (first pulse) and 73 mV (second pulse). The

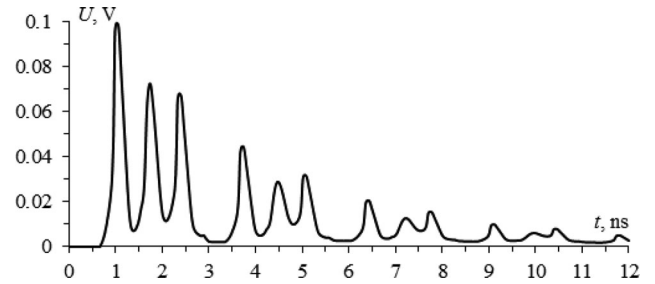


Fig. 12. Output waveform of the MF (simulation with losses).

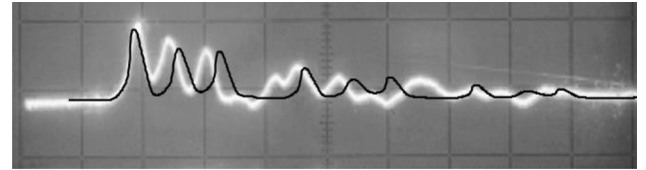


Fig. 13. Output waveforms, obtained in the experiment (white curve) and simulation (black curve). Time and voltage scales are 1 ns/div and 0.1 V/div, respectively.

TABLE I
COMPARISON OF EXPERIMENTAL (E) AND SIMULATED (S) WAVEFORMS

Waveform Parameter	<i>E</i>	<i>S</i>	$ (E - S)/(E + S) $
First pulse amplitude	113 mV	100 mV	6%
Second pulse amplitude	91 mV	73 mV	10%
Difference of delays	0.6 ns	0.71 ns	8%

difference of propagation delays of these pulses is approximately 0.7 ns.

Both experimental and simulated output waveforms on the same scale are presented in Fig. 13. Quantitative comparison of experimental and simulated waveforms with the percent of deviation relative to an average is presented in Table I.

The obtained experimental and simulation waveforms in Fig. 13 have similar shape. According to Table I, the simulated waveform has longer difference of propagation delays and smaller amplitude than the experimental one. The mismatch can be partly caused by the device error of the oscilloscope C9-11 that is 7.5% in the time domain. However, the main reason of such a difference between experimental and simulated waveforms is supposed to be the mismatch of the real dielectric permittivity of the substrate and its mathematical model. The fact is that the mathematical model is averaged over many types of FR-4, while the real substrate is made of the available foiled fiberglass. If the dielectric permittivity of the real substrate is less than that of the averaged FR-4, then it explains the shorter difference of propagation delays in the experiment in comparison with the simulation. This, in turn, leads to the overlapping of the fall of the first pulse and the rise of the second pulse. As a result, the deviation of the second pulse amplitude is more than that of the first one. Thus, the experiment proves the validity of the simulation.

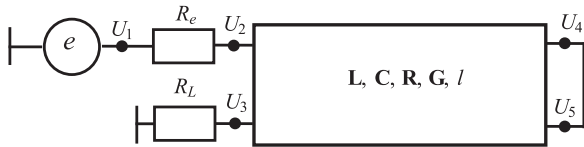
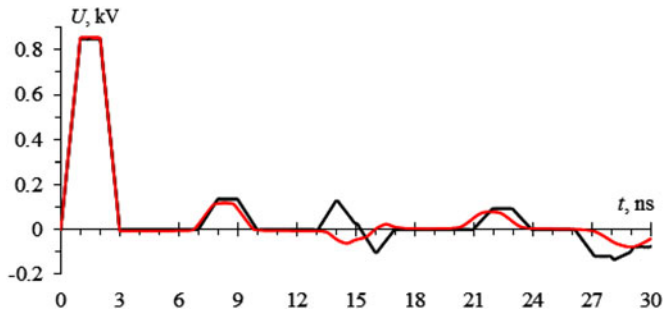
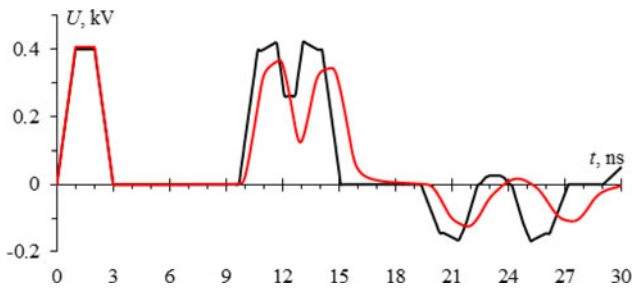


Fig. 14. Circuit diagram of the ML.

Fig. 15. Output waveforms of the ML with $s = 15$ mm, $h = 0.5$ mm with (—) and without (---) losses. Lossless waveform is adapted from [10].Fig. 16. Output waveforms of the ML with $s = 1$ mm, $h = 6$ mm with (—) and without (---) losses. Lossless waveform is adapted from [10].

V. TURN OF ML

In this section, we consider a structure having the same cross section (see Fig. 2) but another circuit diagram, which is shown in Fig. 14. Essentially, it is a turn of a ML, which represents another approach to the protection against UWB pulses. The output of the structure corresponds to the U_3 node.

Output waveform of the ML with initial parameters of the cross section ($s = w = d = 15$ mm, $h = 0.5$ mm, $\epsilon_r = 4$, and $l = 1$ m) is shown in Fig. 15. The obtained waveform is the sum of the signal itself, passed along the first and the second half-turns of ML, and the crosstalk from the input signal rise and fall. Initial s and h values provide a close coupling, and consequently, the amplitude at the output (0.85 kV) is close to the input pulse amplitude (1 kV). As can be seen from Fig. 15, the losses do not influence the crosstalk amplitude.

In order to reduce the coupling (and thus decrease the amplitude of the crosstalk), we can increase the h value and decrease the s value. For example, the output waveform of the ML with changed parameters ($s = 1$ mm, $h = 6$ mm) is shown in Fig. 16.

Although the reduction of the coupling leads to the decrease of the crosstalk amplitude, it also leads to the increase of the delayed pulses amplitude. The optimal case is when these

amplitudes are equal as can be seen in Fig. 16 for the lossless curve, where the amplitude is 0.4 kV and the attenuation coefficient is 2.5. In the case with losses, the amplitude of delayed pulses in Fig. 16 is smaller. The amplitude of the output signal can be slightly decreased further by decreasing of coupling.

VI. CONCLUSION

In this paper, the UWB pulse decomposition in simple structures for low cost and effective protection is described. Detailed simulations for lossless and frequency-dependent losses are presented. The validity of the simulation is confirmed by the experiment.

For the first time, it was demonstrated that the asymmetrical MF without resistors can have attenuation coefficient 2.7 times higher (19 compared to 7) than the MF with resistors for the same parameters of the cross section. It is shown that changing the cross-section parameters and length of the MF without resistors may increase the attenuation coefficient up to 55.

Another principle of the UWB pulse decomposition based on the widely used ML is shown for the same cross section. For this approach, the attenuation coefficient 2.5 is obtained. Despite this, it is much smaller than that of the MF and the ML can be much shorter than the MF, at least due to the two-way against one-way propagation from input to output. Moreover, the use of combined connection of the MF and the ML structures is possible and can be convenient and effective due to the same cross section used. Note that for this cross section, the use of the simplest double-layer PCB is sufficient, while the use of multilayer PCB can simplify both one-stage and multistage realizations.

For each structure, the influence of losses and the possibility of improvement of protection are shown. However, the losses may be more considerable for shorter UWB pulses, while in this paper the UWB pulses parameters are assumed to be constant.

The influence of the proposed structures on the wanted signal is the question of a separate research. Here we note only that this influence depends on the type of the protected circuit (type of the wanted signal) and it is different for MF and ML: the MF has a lowpass amplitude frequency characteristic, and its bandwidth can be adjusted by the choice of its parameters, whereas the characteristic of ML has the all-pass character.

In this paper, the numerical simulation has been used to demonstrate the essence of the proposed design principles. However, due to the simplicity of the considered cross section and structures, the analytical expressions can be used to calculate coupled line parameters and waveforms. Use of these expressions will allow to obtain analytically the optimal parameters giving the best characteristics of protective structures under design constrains.

Results of this paper contribute to a significant reduction of the MF cost and to the implementation of the new principles of protection. New devices based on the described principles will be reliable, cheap, and radiation resistant due to the absence of any lumped components.

REFERENCES

- [1] E. Genender, H. Garbe, and F. Sabath, "Probabilistic risk analysis technique of intentional electromagnetic interference at system level," *IEEE Trans. Electromagn. Compat.*, vol. 56, no. 1, pp. 200–207, Feb. 2014.
- [2] A. M. Zabolotsky, T. R. Gazizov, A. G. Bova, and W. A. Radasky, "Dangerous pulse excitation of coupled lines," in *Proc. 17th Int. Zurich Symp. Electromagn. Compat.*, Zurich, 2006, pp. 164–167.
- [3] F. Brauer and J. Haseborg, "SPICE simulations and measurement techniques for protection circuits against UWB and HPM signals," in *Proc. Book Abstracts EUROEM 2008*, p. 23.
- [4] T. R. Gazizov, A. M. Zabolotsky, and I. E. Samotin, "Modal decomposition of UWB pulse in power cable structures: Simple experiment showing useful possible applications," in *Proc. Book Abstracts EUROEM*, 2008, p. 62.
- [5] T. R. Gazizov, I. E. Samotin, A. M. Zabolotsky, and A. O. Melkozerov, "Design of printed modal filters for computer network protection," in *Proc. 30th Int. Conf. Lightning Protection*, 2010, pp. 1246–1–1246-3.
- [6] T. R. Gazizov, A. M. Zabolotsky, A. O. Melkozerov, E. S. Dolganov, and P. E. Orlov, "Improved design of modal filter for electronics protection," in *Proc. 31st Int. Conf. Lightning Protection*, 2012, pp. 1–4.
- [7] T. R. Gazizov, A. M. Zabolotsky, and E. S. Dolganov, "Modal filter as a device for electrostatic discharge protection of onboard computers and control units of space vehicles," *Russian Phys. J.*, vol. 55, pp. 282–286, 2012.
- [8] A. M. Zabolotsky and A. T. Gazizov, "Simulation of ultra-wide band pulse propagation in asymmetrical modal filter for power network protection," *Int. J. Circuits, Syst. Signal Process.*, vol. 9, pp. 68–74, 2015.
- [9] A. T. Gazizov and A. M. Zabolotsky, "UWB pulse decomposition in asymmetrical modal filter with different boundary conditions," in *Proc. 2015 Int. Siberian Conf. Control Commun. (SIBCON)*, 2015, pp. 1–3.
- [10] A. T. Gazizov, A. M. Zabolotsky, and O. A. Gazizova, "Printed structures for protection against UWB pulses," in *Proc. 16th Int. Conf. Young Spec. Micro/Nanotechnol. Electron. Devices EDM*, 2015, pp. 120–123.
- [11] A. T. Gazizov, "Simple printed structures for low-cost and effective protection against UWB pulses," in *Proc. ASIAEM*, 2015, pp. 1–3.
- [12] Q. Zhang, J. Bandler, and C. Carloz, "Design of dispersive delay structures formed by coupled C-sections using predistortion with space mapping," *IEEE Trans. Microw. Theory Tech.*, vol. 61, no. 12, pp. 4040–4051, Dec. 2013.
- [13] R. S. Surovtsev, A. V. Nosov, and A. M. Zabolotsky, "Simple method of protection against UWB pulses based on a turn of meander microstrip line," in *Proc. 16th Int. Conf. Young Spec. Micro/Nanotechnol. Electron. Devices EDM*, 2015, pp. 175–177.
- [14] R. S. Surovtsev, T. R. Gazizov, and A. M. Zabolotsky, "Pulse decomposition in the turn of meander line as a new concept of protection against UWB pulses," in *Proc. 2015 Int. Siberian Conf. Control Commun.*, pp. 1–5.
- [15] A. R. Djordjevich, R. M. Biljic, V. D. Likar-Smiljanic, and T. K. Sarkar, "Wideband frequency-domain characterization of FR-4 and time-domain causality," *IEEE Trans. Electromagn. Compat.*, vol. 43, no. 4, pp. 662–666, Nov. 2001.
- [16] S. P. Kuksenko, T. R. Gazizov, A. M. Zabolotsky, R. R. Ahunov, R. S. Surovtsev, V. K. Salov, and E. V. Lezhnin, "New developments for improved simulation of interconnects based on method of moments," in *Proc. 2015 Int. Conf. Modelling, Simul. Appl. Math.* (Advances in Intelligent Systems Research (ISSN 1951-6851)), Aug. 23–24, Phuket, Thailand, pp. 293–301.
- [17] T. R. Gazizov, "Analytic expressions for mom calculation of capacitance matrix of two dimensional system of conductors and dielectrics having arbitrary oriented boundaries," in *Proc. 2001 IEEE EMC Symp.*, pp. 151–155.
- [18] J. R. Griffith and M. S. Nakhla, "Time-domain analysis of lossy coupled transmission lines," *IEEE Trans. Microw. Theory Tech.*, vol. 38, no. 10, pp. 1480–1487, Oct. 1990.
- [19] T. R. Gazizov, "Calculation of a capacitance matrix for a two-dimensional configuration of conductors and dielectrics with orthogonal boundaries," *Russian Phys. J.*, vol. 47, p. 326, 2004.
- [20] R. F. Harrington and C. Wei, "Losses on multiconductor transmission line in multilayered dielectric media," *IEEE Trans. Microw. Theory Tech.*, vol. 32, no. 7, pp. 705–710, Jul. 1984.
- [21] M. R. Scheinfein and O. A. Palusinski, "Methods of calculation of electrical parameters for electronic packaging applications," *Trans. SCS*, vol. 4, no. 3, pp. 187–254, Jul. 1987.
- [22] I. E. Samotin, "Alignment condition of the pulse amplitudes on the output of the modal filter," (in Russian), *Technol. EMS*, vol. 35, pp. 31–34, 2010.



Alexander Talgatovich Gazizov is currently working toward the B.S. degree at the National Research Tomsk Polytechnic University, Tomsk, Russia.

He is a Junior Research Fellow at the Scientific Research Laboratory "Security and Electromagnetic Compatibility of Radioelectronic Equipment," Tomsk State University of Control Systems and Radioelectronics (TUSUR), Tomsk. He is the author or coauthor of 20 scientific papers.



Alexander Mikhailovich Zabolotsky received the Engineering degree and the Ph.D. degree from Tomsk State University of Control Systems and Radioelectronics (TUSUR), Tomsk, Russia, in 2004 and 2010, respectively.

He is currently a Senior Research Fellow at TUSUR. He is the author or coauthor of 164 scientific papers, including 6 books.



Talgat Rashitovich Gazizov was born in 1963. He received the Engineering degree, the Ph.D. degree, and the D.Sc. degree from Tomsk State University of Control Systems and Radioelectronics (TUSUR), Tomsk, Russia, in 1985, 1999, and 2010, respectively.

His current research interests includes signal integrity problem. He is the author or coauthor of 244 scientific papers, including 10 books.